IEEE Photonics Journal
An IEEE Photonics Society Publication

Open Access

Self-Oscillating Parametric Optical Frequency Comb Generation Using an Electroabsorption Modulated Laser-Based Optoelectronic Oscillator

Volume 11, Number 4, August 2019

Yumin Cheng
Juanjuan Yan
Siyu Zhao

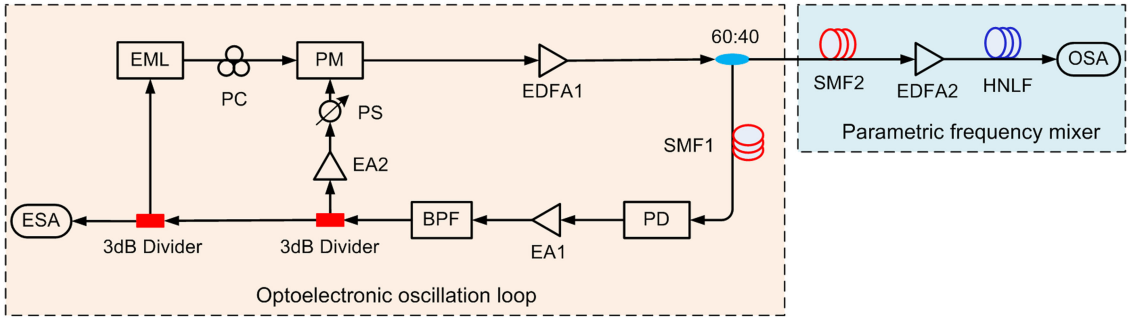

DOI: 10.1109/JPHOT.2019.2928819

Self-Oscillating Parametric Optical Frequency Comb Generation Using an Electroabsorption Modulated Laser-Based Optoelectronic Oscillator

Yumin Cheng, Juanjuan Yan, and Siyu Zhao

School of Electronic and Information Engineering, Beihang University, Beijing 100191, China

DOI:10.1109/JPHOT.2019.2928819

Manuscript received May 27, 2019; revised June 28, 2019; accepted July 11, 2019. Date of publication July 15, 2019; date of current version July 26, 2019. This work was supported by the National Natural Science Foundation of China under Grants 61771029 and 61201155. Corresponding author: Juanjuan Yan (e-mail: yanjuanjuan@buaa.edu.cn).

Abstract: A scheme for parametric optical frequency comb (OFC) generation using an electroabsorption modulated laser (EML) based optoelectronic oscillator is proposed and experimentally demonstrated. A phase modulator is cascaded with EML in the oscillating loop. In addition, the phase modulated laser is used as pump seeds for the parametric frequency mixer. In the mixer, a 100-m single-mode fiber is employed to compress the pump pulses, and the parametric process is stimulated in a 200-m-high nonlinear fiber (HNLF) with flat normal dispersion. In our experiments, a 10-GHz radio frequency signal with a side-mode suppression radio of 47 dB and a single-sideband phase noise of −109.89 dBc/Hz at 10 kHz offset is obtained. When the pump power injected into HNLF is 28 dBm, a 10-tone parametric OFC with a 5-dB power variation and spacing equal to the oscillation frequency is generated.

Index Terms: Parametric optical frequency comb, electroabsorption modulated laser, optoelectronic oscillator.

1. Introduction

Optical frequency combs (OFCs) with high coherence, great flatness and stability are attractive for diverse applications such as time and frequency metrology [1], arbitrary waveform synthesis [2], wavelength division multiplex (WDM) communication [3] and so on [4]. The method of external modulation of continues-wave (CW) light has been frequently used to generate OFCs owing to its advantages of adjustability and stability [5]–[7]. However, it has been found that the number of comb lines generated with this method is determined by the modulation depth. And more electro-optical phase modulators (PMs) have to be cascaded to produce more frequency lines [8]. Recently, it has attracted more and more attention to achieve spectrum expansion and flatness enhancement in OFC generation by using parametric multicasting mixers [9]–[12]. And the traditional parametric mixers are pumped by two free-running continuous-wave (CW) lasers [9], leading to the linewidth of comb lines increasing quadratically with the line order [10]. To cancel this spectral linewidth broadening and noise growth in parametric OFC generation, phase-correlated pump seeds are required. In [10], two distributed-feedback (DFB) slave lasers injection locked by two sidebands of a phase modulated CW laser are employed to seed parametric mixers. Alternatively, cascaded

Mach-Zehnder modulator (MZM) and PM are used to provide pumps for the generation of broadband parametric OFCs in [11], [12]. Consequently, in these works, a radio-frequency (RF) signal source is needed to drive the modulators. On the other hand, it has been found that the phase noise of the phase/intensity-modulated laser shows a linear increase with the sideband order and that the slope corresponds to the amount of the phase noise in the external RF synthesizer [13]. As a result, the phase noise performance of the comb lines generated by using electro-optical modulators (EOMs) may also be poor, especially when a high frequency RF signal used. This is because the output signals of a high-frequency RF synthesizer are usually derived from frequency multiplication of a low-frequency quartz oscillator, which also multiplies the phase noise [14]. To overcome this limitation, some schemes of self-oscillating OFC generators have been proposed and experimentally demonstrated [14]–[16]. In these works, an EOM-based OFC generator is embedded in an optoelectronic oscillator (OEO) topology, where the generated optical comb is photo-detected to produce a microwave output to drive the modulators. So, no frequency synthesizer is required, and the phase noise of the RF driving signal is low and frequency-independent [14]. An MZM and a PM are cascaded in the oscillation loop to generate optical frequency combs in [15], while a dual-drive MZM is used in [16]. Large-signal RF inputs are fed back to these modulators to generate more sidebands [8], [16]. Alternatively, a monolithic OFC generator consisting of a PM and a Fabry-Perot (FP) resonator has been employed to replace the conventional EOMs in the OEO loop [14]. For these schemes, a CW laser is used to provide carriers for the modulator, and a larger coupling loss between the two components is usually introduced.

In contrast to traditional $LiNbO_3$ MZMs, electroabsorption modulators (EAMs) have the advantages of fast response and low power consumption. Also, their insertion loss has been demonstrated to be as low as 5.2 dB at 1550 nm [17]. An EAM has been employed in a dual-loop OEO, and the generated electrical signal is used to drive two PMs outside of the OEO loop to produce chirped pulses for the generation of short pulses [18]. Meanwhile, EAMs have another more attractive advantage over MZMs, i.e., they can be integrated with lasers easily in a quite small size and have been widely used as transmitters in long distance and high-speed optical fiber communication systems [19]. So, in our work, we replace a CW laser and an MZM or an EAM in an OEO loop with an electroabsorption modulated laser (EML) to design a self-starting parametric OFC generator. In this generator, a PM cascaded with the EML is also embedded in the oscillation loop to produce chirped pulses. As a result, the pulses have a higher stability than those generated by use of the scheme with PMs at outside of the oscillation loop in [18]. And then these chirped pulses are compressed in a length of single mode fiber (SMF) and then launched into a section of highly nonlinear fiber (HNLF) to realize parametric mixing after optical amplification. In our experiments, a 10-GHz RF signal with a side-mode suppression radio (SMSR) of 47 dB and a single side band (SSB) phase noise of -109.89 dBc/Hz at 10 kHz offset is generated. After pulse compression and parametric mixing, a 10-tone comb with a spacing of 10 GHz in a power variation of 5 dB is obtained.

Compared with the existing OFC generators based on external modulation [5]–[7], [10]–[13], our scheme has the advantage of no need of a microwave source, and it can also be adjustable if an electrical bandpass filter (BPF) with a tunable central frequency is used in the oscillation loop. Also, compared with the methods of self-oscillating OFC generation [14]–[16], [18], the coupling loss between the CW laser and the modulator is reduced by using of EML, and the driving power for PM is decreased since the spectrum expansion can be achieved outside the loop with parametric process. So, our scheme also has the advantages of large bandwidth and low power consumption.

2. Principle

The schematic diagram of our proposed parametric frequency comb generator based on an optoelectronic oscillator is shown in Fig. 1. It consists of an optoelectronic oscillation loop and a parametric frequency mixer. In the optoelectronic oscillation loop, the laser from an EML is phase modulated, and a polarization controller (PC) is used to align the polarization of the laser to the PM. The output laser of the PM is amplified by an Erbium-doped optical fiber amplifier (EDFA1) to control the gain of the optical loop. Then, a part of the amplified signal is delayed with a section

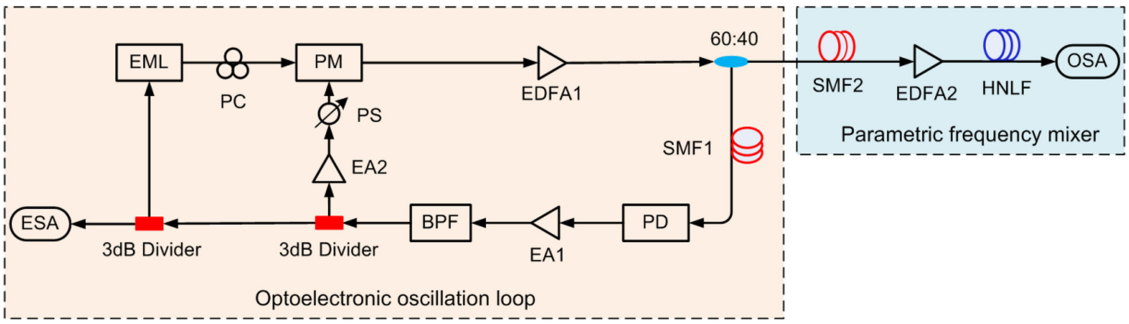

Fig. 1. Schematic diagram of the proposed optical frequency comb generator using an electroabsorption modulated laser based OEO. EML: electroabsorption modulated laser. PC: phase controller. PM: phase modulator. EDFA: erbium-doped fiber amplifier. SMF: single mode fiber. HNLF: high nonlinear fiber. OSA: optical spectrum analyzer. PD: photo-detector. EA: electrical amplifier. BPF: bandpass filter. PS: phase shifter. ESA: electrical spectrum analyzer.

of standard single mode fiber (SMF1) and detected by a photo-detector (PD). The output electrical signal from PD is amplified with an electrical amplifier (EA1), and a BPF with a narrow bandwidth is adopted to suppress the unwanted transmission resonances. The output signal from BPF is fed back to drive the EML and PM to form a closed oscillation loop. The oscillation frequency is determined by the center frequency of the BPF. The power fluctuation of the generated OFC in the loop can be improved by adjusting another electrical amplifier (EA2) and a RF phase shifter (PS).

The output power of the EML depends on voltage applied to the EAM. If the voltage is V_{in}, the output optical power of the EML is described as [19]:

$$P_{EML\_out} = P_{\max}\left\{(1-\varepsilon_{\max})\exp\left[-\left(\frac{V_{in}}{V_a}\right)^a\right]+\varepsilon_{\max}\right\} \tag{1}$$

where V_a and a are fitting parameters, $P_{\max}$ is the output optical power of the EML with zero modulation voltage applied, and $\varepsilon_{\max}$ is the maximum extinction obtained by the modulator. When the feedback signal with an amplitude of V_1 and a frequency of ω is applied to the EML, V_{in} is expressed as,

$$V_{in} = V_{bias} + V_1\cos(\omega t) \tag{2}$$

where V_{bias} is the direct current (DC) bias voltage. The output electrical field of the EML is [19],

$$E_{EML\_out} = \sqrt{P_{EML\_out}}\exp\left[j\frac{\alpha_H}{2}\ln(P_{EML\_out})\right] \tag{3}$$

where α_H is the chirp parameter. This signal laser is then phase modulated, and the output electrical field of the PM can be described as,

$$E_{PM\_out} = E_{EML\_out}\exp\left[j\frac{\pi V_2\cos(\omega t+\theta)}{V_\pi}\right] \tag{4}$$

where V_π and V_2 are respectively the half-wave voltage and the amplitude of the driving signal applied to PM, and θ is the relative phase shift between the signals driving EML and PM. From Eq. (3) and Eq. (4), it can be seen that chirped pulses are produced when the oscillation is achieved. After optical amplification, a portion of the pulse laser is injected into SMF1 and detected with PD to form an oscillation loop. Another portion of the laser is launched into the parametric frequency mixer, where the pulses are compressed when propagating in SMF2 due to the interactions between dispersion and chirps. After optical amplification with EDFA2, the compressed pulses are coupled into a length of HNLF to stimulate multistage four-wave-mixing (FWM), and more parametric sidebands are generated. An efficient parametric OFC generation relies on the pump power and the degree of phase-matching that can be achieved across the operating bandwidth [9]. Here, a section of HNLF

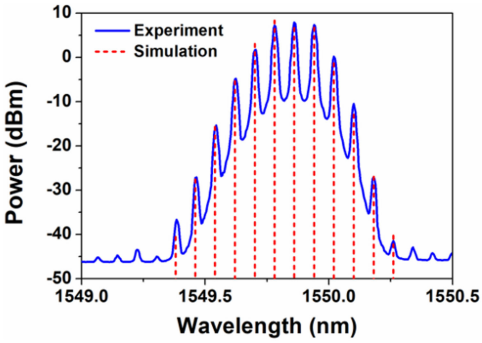

Fig. 2. The measured (solid line) and the simulated (dash line) output spectrum of PM.

with flat normal dispersion is adopted to ensure phase-matching over a broadened spectral span and suppress the parametric noise induced by modulation instability [9].

3. Experimental Results and Discussions

Based on the above principle of operation, proving experiments and simulation are performed. In the experiments, an EML (CyOptics LIM400) with a 3-dB bandwidth of 30 GHz working at 1549.87 nm is employed. It is biased at 1.5 V, and the output power is 2.7 dBm. The PM (Covega) has a 3-dB bandwidth of 10 GHz and a half-wave voltage of 3.5 V. The gain of EDFA1 is 16 dB. The amplified signal is split with a 60/40 optical coupler. 40% of the signal is injected into SMF1 and then photoelectrically detected by a PD with a 3-dB bandwidth of 30 GHz. The generated electrical signal is amplified with EA1 and bandpass filtered by a BPF centered at 10 GHz with a 3-dB bandwidth of 150 MHz. So, a 10-GHz RF signal is produced, and it is feedback to drive the EML and the PM. In the loop, the length of SMF1 is 1km for a trade-off: a longer fiber would take the phase noise spurs forward with no significant improvement for the lower frequency part of SSB phase noise spectrum [20]. In the parametric mixer, 60% of the output signal from EDFA1 is launched into SMF2 with a length of 100 m, and then amplified with EDFA2 (Amonics) to act as parametric pumps. Consequently, multistage FWM occurs in the 200-m HNLF, and a parametric frequency comb is created. The nonlinear coefficient of HNLF is larger than 10 $W^{-1}km^{-1}$, and its dispersion coefficient and dispersion slope are respectively -2.569 ps/nm/km and 0.005 $ps/nm^2/km$. In the experiments, both an electrical spectrum analyzer (ESA: CETC41 AV4051E) and an optical spectrum analyzer (OSA: YOKOGAWA AQ6375B) are utilized to monitor the electrical signal and the optical signal in the OFC generator.

For our used EML (LIM400) in the experiments, its output power is measured when adjusting the DC bias voltage. The measured results are fitted with Eq. (1), and these results give values of $P_{max} = 4.5$ mW, $\varepsilon_{max} = 1/27$, $V_a = 1.5$ V and $a = 2.5$. The measured output spectrum of PM is shown in Fig. 2, and simulated results are also presented in the figure as a comparison. It can be seen that the two results exhibit a good agreement, and more sidebands are observed, which shows a stable oscillation realized. The spectrum is asymmetrical due to the phase shift between the two driving signals for EML and PM.

Fig. 3 shows the spectra of generated RF signal observed by ESA. A spectral line of 10 GHz is clearly observed in the span of 20 GHz in Fig. 3(a). When the span is set to be 1 MHz and the resolution bandwidth (RBW) is 1 kHz, some side-modes are observed due to non-ideal mode selection. The mode spacing is 200 kHz, which corresponding to the free spectral range (FSR) of the OEO with a 1-km SMF1 in the loop. The side mode suppression ratio (SMSR) is about 47 dB, and according to Fig. 3(b), the oscillating frequency is measured to be 9.98404 GHz.

The SSB phase noise of the generated oscillation signal is evaluated with the signal analyzer. The measured results are shown in Fig. 4. When the offset frequencies are below 10 kHz, the

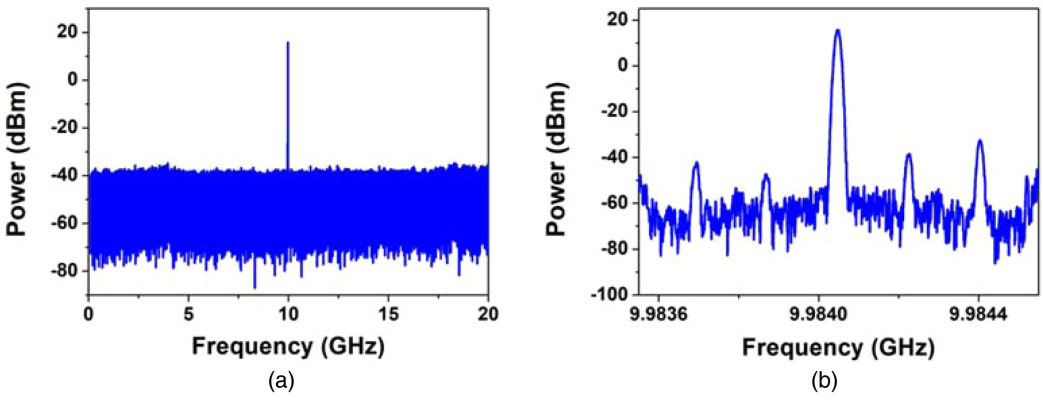

Fig. 3. The measured electrical spectra of the generated 10 GHz-oscillation signal in a span of (a) 20 GHz and (b) 1 MHz.

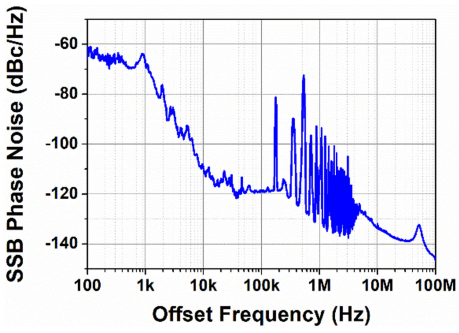

Fig. 4. Single-sideband phase noise of the generated RF signal versus offset frequency.

phase noise is dominated by the EML frequency noise and the flicker noise from PD and electrical amplifiers [21]. Meanwhile, the laser frequency noise is converted to phase noise due to dispersion in SMF1 [20], which results in fluctuations in the low offset frequency range. It can also be found that there are several spurs at offset frequencies of multiple 200 kHz corresponding to the FSR of the OEO. The SSB phase noise at 10 kHz offset is −109.89 dBc/Hz. This performance can be further improved by using low noise electrical amplifiers or a dual-loop configuration [20], [21].

To evaluate the stability of the generated electrical signal, its time jitter, σ_j is calculated by integration of the SSB phase noise,

$$\sigma_j = \frac{1}{2\pi f_{RF}} \sqrt{2 \int_{f_1}^{f_2} L(f) df} \tag{5}$$

where f_{RF} is the frequency of the generated RF signal, and $L(f)$ is the SSB phase noise spectral density. The integral range is determined by f_1 and f_2. When the frequency range is from 100 Hz to 1 MHz, the timing jitter is 909 fs and 33 fs from 4 MHz to 80 MHz of the ITU-T specified range [22]. So, it can be seen that the noise at lower offset frequency mainly contributes to the jitter. This timing jitter is higher than that in [23], and it can be decreased by using of a narrow linewidth EML and a dual-loop configuration, as applied in [23].

On the other hand, it is notable that the frequency stability of the generated electrical signal with this OEO is also affected by the center frequency drifting of the BPF and the sensitivity of the optical link to the temperature and vibration. A passive cavity BPF is used in our experiments, and its center frequency is insensitive to the temperature, however, the mode hopping exerts an influence on the long-term stability of the OEO for the reason that the bandwidth of the BPF is larger than the mode

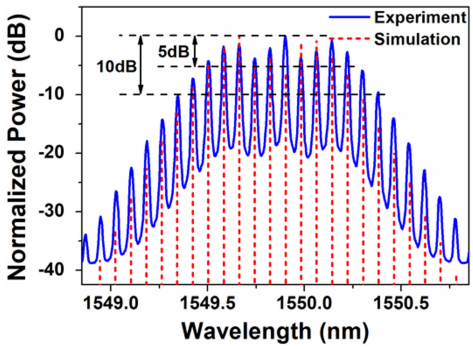

Fig. 5. The experiment (solid line) and simulation (dash line) results of the generated parametric OFC when using 100-m SMF2 for pulse compression.

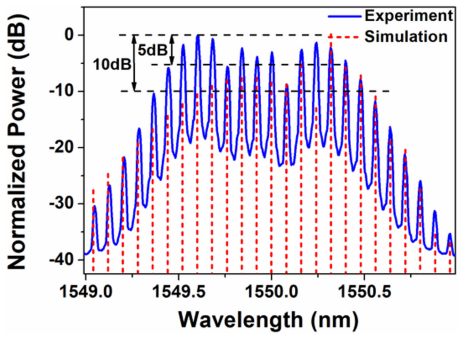

Fig. 6. The experiment (solid line) and simulation (dash line) results of the generated parametric OFC when using 1-km SMF1 in the loop as a pulse compressor.

spacing. Some approaches can be applied to further stabilize the OEO, e.g., using a BPF with a narrower bandwidth and placing this OEO in a temperature controller.

For the parametric frequency mixer, when the power launched into HNLF is 28 dBm, the generated parametric OFC is shown in Fig. 5. As can be seen, a 10-tone frequency comb with a 5-dB power deviation is achieved. The comb line spacing is equal to the oscillation frequency. The power variation can be improved with precise mixer dispersion engineering, e.g., tension-engineered dispersion management [9]. Also, more comb lines can be generated by increasing the pump power or cascading more stages of parametric frequency mixer. In our study, the evolutions of phase modulated pulses in SMF and HNLF are also simulated by solving nonlinear Schrödinger equation (NLSE) with the split-step Fourier method [24]. The simulation parameters are consistent with those in the experiments. As a comparison, the simulated results are also plotted in Fig. 5. It can be seen that the experimental results agree well with the theoretical results in the whole. However, the difference between the two results can still be observed, which is mainly resulted from two facts. One is that the noise including that induced by EML linewidth and amplified spontaneous emission (ASE) noise arising from the two EDFAs is not taken into account in the simulation. The other fact is that a deviation is also induced when solving the equation of NLSE with the split-step Fourier method.

On the other hand, it is worth noting that SMF1 in the loop can also be used for pulse compression in the mixer, and this experiment is performed by connecting the 60:40 coupler with the output of SMF1. 40% of the laser is detected with PD, and the 60% is injected into HNLF after amplification with EDFA2. When the pump power launched into HNLF is 28 dBm, the comb shown in Fig. 6 is observed. The power variation in this case is deteriorated, compared with the spectrum in Fig. 5, though more comb lines are produced within a 10-dB power fluctuation. Similarly, the simulation

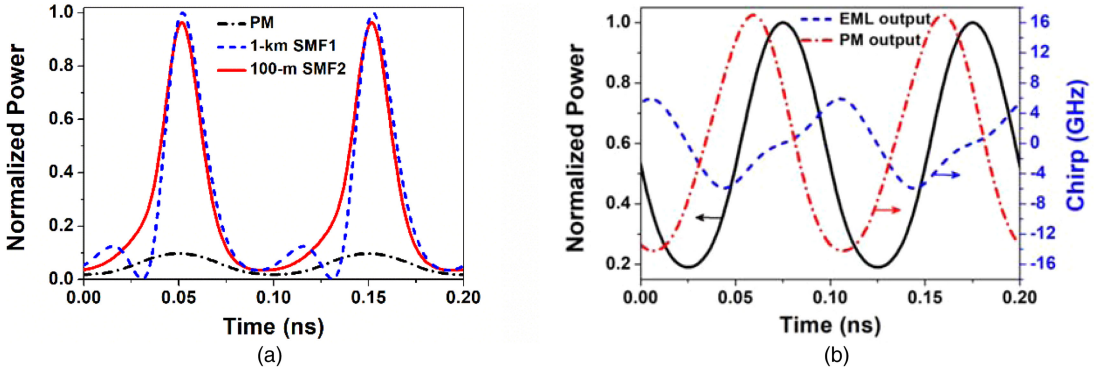

Fig. 7. The simulated results, (a) the pulses output from PM (dash dot line), 1-km SMF1 (dash line) and 100-m SMF2 (solid line); (b) waveform (solid line) and frequency chirps of the output signal from EML (dash line) and PM (dash dot line).

results are also presented in Fig. 6, where more obvious deviation between the experimental results and theoretical results is observed. Besides the reasons listed above, the use of a longer SMF1 for pulse compression resulted in a slightly increased deviation when solving NLSE with the split-step Fourier method, and the deviation is increased again when simulating the pulse propagation in HNLF.

To give an insight into the relationship between the spectral flatness and the waveform shape, more simulation results are presented in Fig. 7. The pulses at the outputs of PM, SMF1 and SMF2 are given in Fig. 7(a). As expected, the pulses are compressed due to the interaction of chirps and fiber dispersion after propagating in SMF. It can be found that when the 1-km SMF1 in the oscillation loop is used for pulse compression, the pulses shown in dash line have the highest peak power, and all the pulse amplitudes in Fig. 7(a) are normalized with this peak power. So, owing to the higher the peak power, more comb tones generated in this case. However, pedestals are observed in the compressed pulses for the phase modulated pulses have both positive and negative chirp [25]. And the pedestals result in the spectral ripples in the generated OFC shown in Fig. 6. Meanwhile, it can also be seen that the compressed pulses are unsymmetrical. This is because the positive chirp of the phase modulated pulses is higher than the negative chirp, as shown in dash dot line in Fig. 7(b). And this asymmetry in frequency chirp is due to the contribution of EAM plotted in dash line. Here, the frequency chirp is calculated by [26]

$$\Delta\nu(t) \equiv \frac{1}{2\pi}\frac{\partial\varphi(t)}{\partial t} \tag{6}$$

where $\varphi(t)$ is the electrical field phase of the considered pulses. When the 100-m SMF2 is employed, the pulses shown in the solid line in Fig. 7(a) are also compressed, compared with those output from PM shown in dash dot line. In this case, no pedestals are observed in the compressed pulses due to a shorter fiber used for the interaction between chirps and dispersion, and the corresponding spectral flatness is improved, as shown in Fig. 5.

This consistency between the time domain and frequency domain can be explained by time-to-frequency (TTF) conversion, which is based on the theory of time-lens, i.e., a quadratic phase modulation in time is an analog of a thin lens in space [27]. According to this theory, when an optical pulse enters a time lens, the amplitude of this pulse is mapped from time domain into frequency domain. So, flat-topped pulses accompanied by a strong linear chirp correspond to a flat frequency comb [28], [29]. In Fig. 7(a), parasitic side-lobes with a lower power (dash line) do not experience obvious self-phase modulation and remain the static relative to the main pulse when propagating in HNLF. These static side-lobes interfere with the expanding edges of pulse and cause fast temporal oscillation and excessive chirping [29]. Correspondingly, an excess spectral

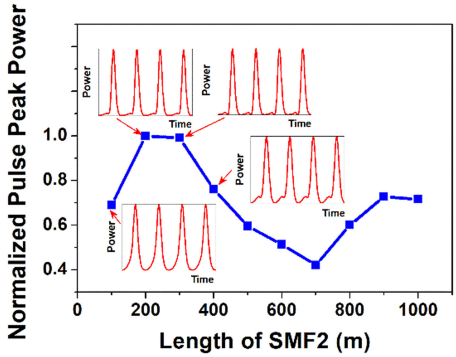

Fig. 8. The simulated results of normalized pulse peak power as a function of length of SMF2, and the waveforms of the compressed pulse are also shown in the insets with the length of SMF2 equal to 100 m, 200 m, 300 m and 400 m.

ripple appears in the entire spectrum range of the parametric OFC. Similarly, ripple-free pulses in time-domain correspond to flat combs in the frequency-domain.

From the discussion shown above, it is implied that a shorter SMF is more suitable for pulse compression in the parametric frequency mixer. However, a longer fiber in the loop contributes to improve the phase noise performance of an OEO in the low frequency part [30]. So, another segment of SMF, i.e., SMF2, is used in our proposed parametric OFC generator. When the length of SMF2 increasing from 100 m to 1 km, the normalized peak power of the compressed pulse is plotted in Fig. 8. When a 200-m SMF2 is used, the pulses are compressed with a highest peak power. However, in this case small pedestals can still be seen, and their amplitudes increase with the length of SMF2 equal to 200 m, 300 m and 400 m, while no pedestal is observed with the length of SMF2 equal to 100 m, as shown in the insets of Fig. 8. As discussed above, the pedestals result in the spectral ripples in the generated parametric OFC. So, as a balance between larger pulse peak power and no pedestal, a 100-m SMF2 is used in our experiments for pulse compression.

4. Conclusion

In summary, we have designed and experimentally demonstrated a self-oscillating parametric OFC generator using an EML-based OEO. The pump seeds for parametric frequency mixing is produced by cascading a PM with the EML in the OEO loop. A 10-GHz oscillating signal with a side-mode suppression radio of 47 dB and a phase noise of −109.89 dBc/Hz at 10 kHz offset is obtained by using this OEO. The parametric frequency mixer is composed of a 100-m SMF and a 200-m HNLF with flat normal dispersion. A 10-tone parametric OFC in the sub-5 dB spectral flatness is experimentally generated when the pump power launched into HNLF is 28 dBm.

Reference

[1] T. Udem, R. Holzwarth, and T. W. Hansch, "Optical frequency metrology," *Nature*, vol. 416, no. 6877, pp. 233–237, 2002.
[2] Z. Jiang, C.-B. Huang, D. E. Leaird, and A. M. Weiner, "Optical arbitrary waveform processing of more than 100 spectral comb lines," *Nature Photon.*, vol. 1, no. 8, pp. 463–467, 2007.
[3] V. Ataie *et al.*, "Ultrahigh count coherent WDM channels transmission using optical parametric comb-based frequency synthesizer," *J. Lightw. Technol.*, vol. 33, no. 3, pp. 694–699, Feb. 2015.
[4] X. Xu *et al.*, "Advanced RF and microwave functions based on an integrated optical frequency comb source," *Opt. Express*, vol. 26, no. 3, pp. 2569–2583, 2018.
[5] T. Sakamoto, T. Kawanishi, and M. Izutsu, "Asymptotic formalism for ultraflat optical frequency comb generation using a Mach–Zehnder modulator," *Opt. Lett.*, vol. 32, no. 11, pp. 1515–1517, 2007.

[6] R. Wu, V. R. Supradeepa, C. M. Long, D. E. Leaird, and A. M. Weiner, "Generation of very flat optical frequency combs from continuous-wave lasers using cascaded intensity and phase modulators driven by tailored radio frequency waveforms," *Opt. Lett.*, vol. 35, no. 19, pp. 3234–3236, 2010.
[7] B. Dai, Z. Gao, X. Wang, H. Chen, N. I. Kataoka, and N. Wada, "Generation of versatile waveforms from CW light using a dual-drive Mach–Zehnder modulator and employing chromatic dispersion," *J. Lightw. Technol.*, vol. 31, no. 1, pp. 145–151, Jan. 2013.
[8] A. J. Metcalf, V. Torres-Company, D. E. Leaird, and A. M. Weiner, "High-power broadly tunable electrooptic frequency comb generator," *IEEE J. Sel. Topics Quantum Electron.*, vol. 19, no. 6, pp. 231–236, Nov./Dec. 2013.
[9] E. Myslivets, B. P.-P. Kuo, N. Alic, and S. Radic, "Generation of wideband frequency combs by continuous-wave seeding of multistage mixers with synthesized dispersion," *Opt. Express*, vol. 20, no. 3, pp. 3331–3344, 2012.
[10] Z. Tong, A. O. J. Wiberg, E. Myslivets, B. P. -P. Kuo, N. Alic, and S. Radic, "Spectral linewidth preservation in parametric frequency combs seeded by dual pumps," *Opt. Express*, vol. 20, no. 16, pp. 17610–17619, 2012.
[11] R. Wu, V. Torres-Company, D. E. Leaird, and A. M. Weiner, "Supercontinuum-based 10-GHz flat-topped optical frequency comb generation," *Opt. Express*, vol. 21, no. 5, pp. 6045–6052, 2013.
[12] S. Yu, F. Bao, and H. Hu, "Broadband optical frequency comb generation with flexible frequency spacing and center wavelength," *IEEE Photon. J.*, vol. 10, no. 2, Apr. 2018, Art. no. 7202107.
[13] A. Ishizawa *et al.*, "Phase-noise characteristics of a 25-GHz-spaced optical frequency comb based on a phase- and intensity-modulated laser," *Opt. Express*, vol. 21, no. 24, pp. 29186–29194, 2013.
[14] X. Xie *et al.*, "Low-noise and broadband optical frequency comb generation based on an optoelectronic oscillator," *Opt. Lett.*, vol. 39, no. 4, pp. 785–788, 2014.
[15] J. Dai *et al.*, "Self-oscillating optical frequency comb generator based on an optoelectronic oscillator employing cascaded modulators," *Opt. Express*, vol. 23, no. 23, pp. 30014–30019, 2015.
[16] G. K. M. Hasanuzzaman, A. Kanno, P. T. Dat, and S. Iezekiel, "Self-oscillating optical frequency comb: Application to low phase noise millimeter wave generation and radio-over-fiber link," *J. Lightw. Technol.*, vol. 36, no. 19, pp. 4535–4542, Oct. 2018.
[17] W.-J. Choi *et al.*, "Low insertion loss and low dispersion penalty InGaAsP quantum-well high-speed electroabsorption modulator for 40-Gb/s very-short-reach, long-reach, and long-haul applications," *J. Lightw. Technol.*, vol. 20, no. 12, pp. 2052–2056, Dec. 2002.
[18] J. Zang *et al.*, "Dual-loop optoelectronic oscillator for generation of stable and ultralow timing-jitter electrical and optical clock," in *Proc. 18th OptoElectron. Commun. Conf. Int. Conf. Photon. Switching*, Tokyo, Japan, 2013, Paper TuPR_4.
[19] R. A. Salvatore, R. T. Sahara, M. A. Bock, and I. Libenzon, "Electroabsorption modulated laser for long transmission spans," *IEEE J. Quantum Electron.*, vol. 38, no. 5, pp. 464–476, May 2002.
[20] O. Lelièvre *et al.*, "A model for designing ultra-low noise single and dual-loop 10-GHz optoelectronic oscillators," *J. Lightw. Technol.*, vol. 35, no. 20, pp. 4366–4374, Oct. 2017.
[21] H. Peng *et al.*, "Tunable DC-60 GHz RF generation utilizing a dual-loop optoelectronic oscillator based on stimulated Brillouin scattering," *J. Lightw. Technol.*, vol. 33, no. 13, pp. 2707–2715, Jul. 2015.
[22] S. Liu *et al.*, "High-channel-count 20 GHz passively mode-locked quantum dot laser directly grown on Si with 4.1Tbit/s transmission capacity," *Optica*, vol. 6, no. 2, pp. 128–134, 2019.
[23] H. Peng *et al.*, "10 GHz low timing-jitter and broadband optical comb generation based on an optoelectronic oscillator," in *Proc. Joint Conf. Eur. Freq. Time Forum IEEE Int. Freq. Control Symp.*, Besancon, France, 2017, pp. 250–252.
[24] G. P. Agrawal, *Nonlinear Fiber Optics*, 3rd ed. San Diego, CA, USA: Academic, 2001.
[25] V. Torres-Company, J. Lancis, and P. Andrés, "Unified approach to describe optical pulse generation by propagation of periodically phase-modulated CW laser light," *Opt. Express*, vol. 14, no. 8, pp. 3171–3180, 2006.
[26] G. P. Agrawal, *Fiber-Optic Communication Systems*, 3rd ed. New York, NY, USA: Wiley, 2002.
[27] J. Azana, N. K. Berger, B. Levit, and B. Fischer, "Spectro-temporal imaging of optical pulses with a single time lens," *IEEE Photon. Technol. Lett.*, vol. 16, no. 3, pp. 882–884, Mar. 2004.
[28] J. Yan, Y. Peng, X. Yao, M. Bai, and Z. Zheng, "Generation of optical frequency combs based on time-to-frequency conversion," *IET Optoelectron.*, vol. 8, no. 3, pp. 149–153, 2014.
[29] V. Ataie, E. Myslivets, B. P.-P. Kuo, N. Alic, and S. Radic, "Spectrally equalized frequency comb generation in multistage parametric mixer with nonlinear pulse shaping," *J. Lightw. Technol.*, vol. 32, no. 4, pp. 840–846, Feb. 2014.
[30] X. S. Yao and L. Malelu, "Optoelectronic oscillator for photonic systems," *IEEE J. Quantum Electron.*, vol. 32, no. 7, pp. 1141–1149, Jul. 1996.